Multi-physics Simulational Analysis of a Novel PCR Micro-Device

Y. Wang[*], K. Pant[*], J. Grover[**], S. Sundaram[*]

[*]CFD Research Corporation, Huntsville, AL, U.S.A., yxw@cfdrc.com
[**]Thermal Gradient, Inc., Pittsford, NY, U.S.A., jgrover@thermalgradient.com

ABSTRACT

This paper presents numerical analysis of a novel PCR microfluidic device that generates different operational temperatures by aligning multiple solid layers of different thermal conductivity. A multi-physics simulation approach that couples fluid flow, heat transfer and PCR chemistry is developed. The modeling framework is capable of predicting the distribution of flow velocity, pressure, temperature, and species concentration in the device, and captures the thermo-fluidic effects on DNA amplification, and thus can be used to assess device performance. Through simulation analysis, we found that sample flow rate substantially affects the PCR amplification factor. Our simulation approach can be readily applied for PCR kinetics studies and virtual prototyping of microfluidic PCR devices for improved design efficiency.

Keywords: PCR, DNA amplification, multi-physics

1 INTRODUCTION

In Polymerase Chain Reaction (PCR), a series of thermocycles are used to amplify the target DNA sequence (template) in the presence of a heat-stable DNA polymerase, two oligonucleotide primers (forward and reverse) specific to the target sequence, and deoxynucleoside triphosphates (dNTPs). While microfluidic devices for PCR amplification have critical applications in biodefense, homeland security, forensics and diagnostics, their efficient design continues to be a challenge. An experiment-only trial-and-error approach can prove to be prohibitively expensive and time consuming, leading to long development cycles. High-fidelity simulation-based design of microfluidic PCR reactors can lead to rapid technology development. Several modeling and simulation efforts have been proposed that focus on either the thermal-fluidic aspect [1, 2] or the reaction kinetics [3] of PCR devices. In this paper, a multi-physics approach that couples fluid flow, heat transfer and PCR chemistry [4] is used to analyze a novel microfluidic PCR device developed by Thermal Gradient (TG), Inc [4]. The simulation not only evaluates the thermal-fluidic fields in the device, but also captures the biochemical response for different operational conditions. Critical design parameters (e.g., flow rate) and their effect on amplification factor are identified and discussed. In general, the present model and simulation methodology can be used for kinetics analysis and optimal design of PCR micro-reactors.

2 METHODS

2.1 PCR Micro-Device

Thermal Gradient (TG) has developed a novel micro-device for fast, continuous PCR thermal cycling in a simple, disposable format. The objective of the project is to establish the need for reaction kinetics modeling for design and performance optimization of the PCR device. A 3D schematic of the TG PCR reactor geometry is shown in Figure 1. The device consists of multiple thermal cycling channels connected serially. Each individual cycle consists of a denaturing channel (maintained at 95°C), an annealing channel (maintained at 55°C), and an extension channel (maintained at 75°C). The different operational temperatures are generated by aligning multiple solid layers of different thermal conductivity in parallel between two heat plates that are held at denaturing and annealing temperatures. The sample containing the DNA template and primers enters the device through a single inlet and undergoes amplification as it traverses through these microfluidic channels and layers.

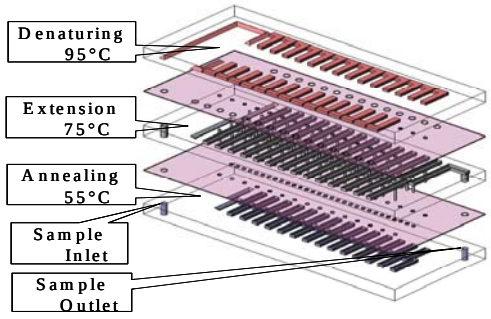

Figure 1. Thermal Gradient (TG)'s PCR micro-device

2.2 Computational Models

Simulations are carried out using CFDRC-developed high-fidelity multi-physics simulation environment, CFD-ACE+, in which three key modules – fluid flow, heat transfer, and chemical kinetics – were invoked. A mathematical description of the modules and the PCR chemistry model is presented next.

2.2.1 Fluidic Models

Viscous, incompressible fluid flow in the microchannels is described by the conservation of mass and momentum equations [6]:

$$\partial\rho/\partial t + \nabla\cdot(\rho u) = 0$$
$$\partial\rho u/\partial t + u\cdot\nabla(\rho u) = -\nabla p + \nabla\cdot(\mu\nabla u) \quad (1)$$

where u, ρ, μ, and p are the fluid velocity, density, dynamic viscosity, and pressure respectively.

2.2.2 Thermal Models

Heat transfer process is computed by numerically solving the total enthalpy equation [6]:

$$\partial\rho h_0/\partial t + u\cdot\nabla(\rho h_0) = \nabla\cdot(k\nabla T) \quad (2)$$

where h_0 is the total enthalpy, k is the thermal conductivity of the fluid. In the present study, the thermal energy transport across solid-fluid interfaces at channel walls is not taken into account. Instead, the microfluidic channel walls are specified at constant temperatures and only the heat transfer within the channels is included.

2.2.3 Species Transport Models

Away from the surface (in the bulk), convective-diffusive species transport equation can be written as [6]

$$\partial c_j/\partial t + u\cdot\nabla c_j = \nabla\cdot(D_j\nabla c_j) + S_j \quad (3)$$

where subscript j represents the jth species in the system; D and c are the mass diffusivity and concentration of the species. The source term S in equation (3) needs to be determined from PCR chemistry models below.

2.2.4 PCR Chemistry Models

The PCR chemistry model used in the present study is based on the model proposed by Hunicke-Smith (1997) [4]. In this model, a total of five major chemical species are used to describe three steps of PCR: denaturing, annealing and extension:

$$\begin{aligned}
&\text{Denaturing} && s_1s_2 \underset{k_D^-}{\overset{k_D^+}{\rightleftarrows}} s_1 + s_2 \\
&\text{Annealing} && s_1 + p_2 \underset{k_A^-}{\overset{k_A^+}{\rightleftarrows}} s_1p_2 \\
& && s_2 + p_1 \underset{k_A^-}{\overset{k_A^+}{\rightleftarrows}} p_1s_2 \\
&\text{Extension} && s_1p_2 \xrightarrow{k_E} s_1s_2 \\
& && p_1s_2 \xrightarrow{k_E} s_1s_2
\end{aligned} \quad (4)$$

where s_1s_2 represents double-stranded DNA (dsDNA), s_1 and s_2 represent its single strands (ssDNA), p_1 and p_2 denote the forward and reverse primers, s_1p_2 and s_2p_1 are the primer-ssDNA complexes. The forward and backward rate constants for denaturing, annealing, and extension are, respectively, given by

$$k_D^+(T) = k_0^+\left(1+\tanh\left[(T-88)/5\right]\right)/2 \quad (s^{-1})$$
$$k_D^-(T) = k_0^-\left(1+\tanh\left[-(T-75)/5\right]\right)/2 \quad (M^{-1}s^{-1}) \quad (5)$$

$$k_A^+(T) = k_1^+\left(1+\tanh\left[-(T-62.5)/5\right]\right)/2 \quad (M^{-1}s^{-1})$$
$$k_A^-(T) = k_1^-\left(1+\tanh\left[(T-66)/5\right]\right)/2 \quad (s^{-1}) \quad (6)$$

$$k_E = k_2\exp\left\{-\left[(T-70)/5\right]^2\right\} \quad (s^{-1}) \quad (7)$$

where T is the temperature in degrees, Celsius (°C); k_0^+, k_0^-, k_1^+, and k_1^- were taken to be as follows: $k_0^+ = 12.5\ s^{-1}$, $k_0^- = 10^6 M^{-1}s^{-1}$, $k_1^+ = 5\times10^6 M^{-1}s^{-1}$, $k_1^- = 10^{-4}s^{-1}$, and $k_2 = 0.32$. Values reported in the literature [3] were used to guide the choice of the reaction parameters, wherever possible. The temperature dependence of the various rate constants is presented in Figure 2. It shows that at desired temperature set points of denaturing and annealing, the forward reaction dominates. The unidirectional extension reaction maximizes around 70°C.

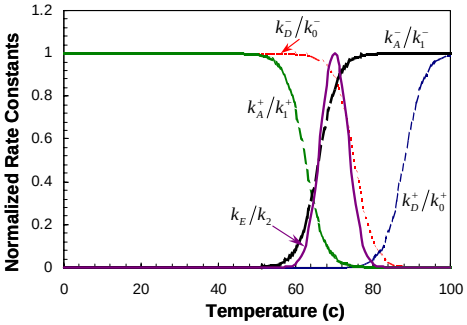

Figure 2. Temperature dependence of rate constants

3 RESULTS AND DISCUSSION

In the present study, a 10-cycle PCR reaction section of the TG PCR micro-device was used. A fully structured computational domain consisting of ~130,000 hexahedral elements was generated. Transport and material properties (density, viscosity, thermal conductivity, etc.) and operational parameters (target and primer concentrations, etc.) were supplied by TG or from best estimation. The values used are summarized in Table 1.

Fluid Parameters		
Density		1000 kg m^{-3}
Dynamic Viscosity		0.001 kg $m^{-1}s^{-1}$
Specific Heat		4106 J $kg^{-1}K^{-1}$
Thermal Conductivity		0.6 W $m^{-1}K^{-1}$
Species Parameters		
P1 & P2	1×10^{-9} m^2s^{-1}	3×10^{-7} M
S1 & S2	1×10^{-10} m^2s^{-1}	0 M
S1P2 & S2P1	1×10^{-10} m^2s^{-1}	0 M
S1S2	1×10^{-10} m^2s^{-1}	5.71×10^{-12} M

Table 1. Properties and operational parameters in simulations

A baseline flow rate of 100 μl/min was used for the calculations. Additional simulations with flow rates of 60 μl/min and 125 μl/min were carried out to investigate the effect of sample flow rate (i.e., throughput) on PCR amplification efficiency. As mentioned previously, heat transfer through solid layers and solid-fluid interface was neglected and only fluid flow, convective heat transfer, species transport and reaction dynamics within channels were included in the analysis.

3.1 Thermal-Fluidic Dynamics

Figure 3 shows the contour plot of the flow velocity magnitude and temperature distribution in the PCR micro-device. As expected, laminar flow dominates due to the microscale channel dimension and low flow velocity (~mm/s).

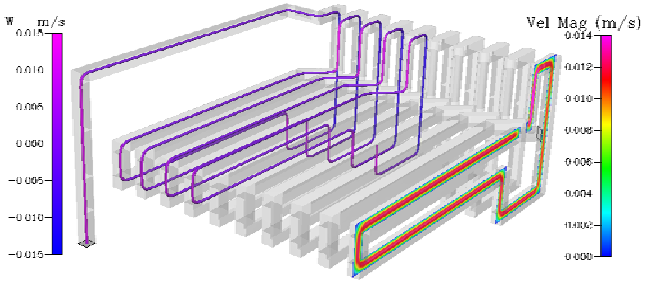

Figure 3. Simulation results of TG PCR device. Contour plot of flow velocity magnitude and stream-tube.

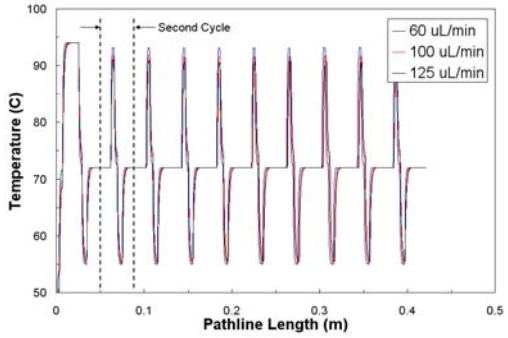

(a)

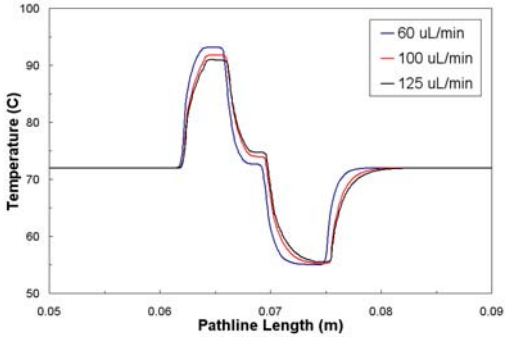

(b)

Figure 4. Temperature variation along a flow pathline (a) All cycles (b) Enlarged view of the second cycle.

The temperature variation in the PCR micro-device along a flow pathline is shown in Figure 4. The pathline is originated at the geometrical center of the sample inlet plane and tracks along the tortuous micro-channel in the device. The centerline fluidic element represents the "worst-case" thermal scenario, as the temperature in the core of the fluid will exhibit the largest deviation from the wall temperature. The results from all three flow rates – 60, 100, 125 μl/min – are presented. Note that thermal equilibrium is largely established for all flow rates considered in this study. There are small spatial discrepancies in the attainment of thermal equilibrium depending on the flow rate and the associated entry length effect, i.e., at higher flow rate the temperature equilibrates slower than at lower flow rates. However, the denaturing, annealing and extension channel lengths are sufficiently long that the fluid exiting the channel has reached the temperature set point for the PCR step to go completion.

3.2 Biochemical (PCR) Dynamics

Surface concentration contours of the dsDNA (s_1s_2) and ssDNA (s_1 is shown here, similar observations were made for s_2) are presented in Figure 5.

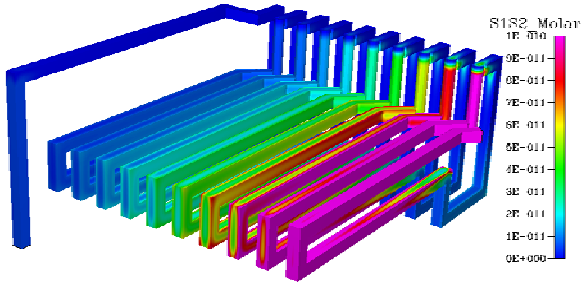

(a)

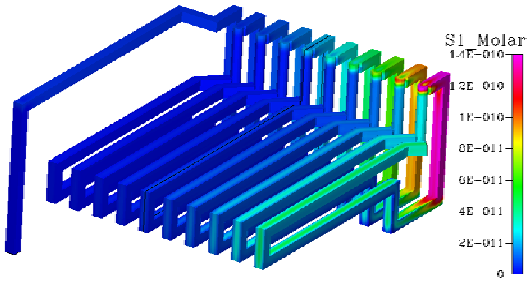

(b)

Figure 5. Simulation results of TG PCR device (a) Concentration distribution of dsDNA (s_1s_2) (b) Concentration distribution of ssDNA (s_1).

It can be seen that the concentration of the dsDNA increases exponentially as the sample traverses down the micro-device. However, not all ssDNA is complexated to the primers in the annealing channel, and a significant amount enters the extension channel. Therefore, the design of annealing and extension channels in the current device can be optimized to improve overall device performance. Another interesting point of note is the cross-sectional non-

NSTI-Nanotech 2007, www.nsti.org, ISBN 1420061844 Vol. 3, 2007

homogeneity of the dsDNA in the device. This makes sense intuitively since the residence time for the ssDNA and primer complex is higher near the walls of the microchannels due to the parabolic flow profile. This means that the extension reaction progresses farther to completion near the corners (in a cross-sectional sense) than in the core of the flow.

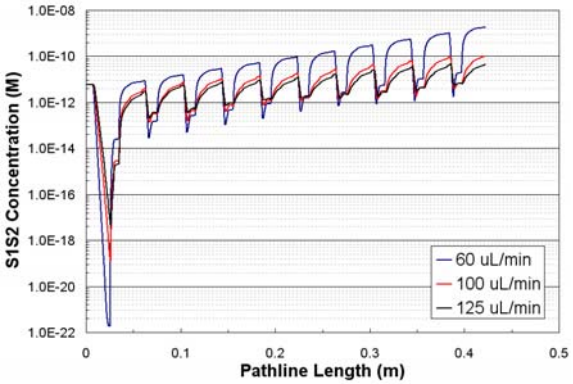

(a)

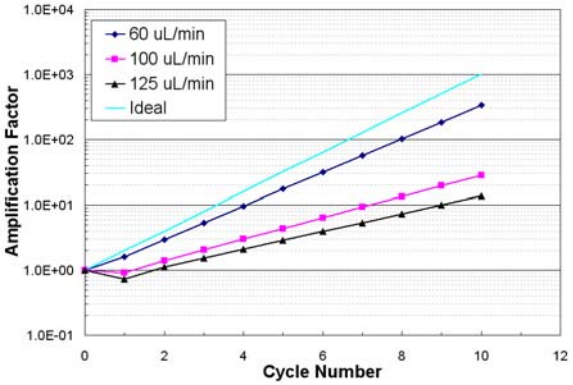

(b)

Figure 6. Concentration and amplification of dsDNA (a) Along the pathline (b) Amplification factor vs. cycle number.

The dsDNA (s_1s_2) concentration along the same flow pathline as the one used for generating temperature distribution in Figure 4 is shown in Figure 6(a). Note that the effect of flow rate on dsDNA is noticeably more pronounced than the effect on temperature distribution. At low flow rates, amplification factors close to the ideal (2 per cycle/loop) are observed whereas at higher flow rates, dsDNA yield exhibits significant non-idealities. However, from an operational standpoint, it is clearly desirable to operate the reactor at high sample throughputs (i.e., high flow rate and short processing time). The computational framework developed in the present study can be used to evaluate these design trade-offs in a systematic manner and lead to rational device design.

4 CONCLUSION

In this paper, we have investigated a novel PCR micro-device using multi-physics simulations. Fluid flow, heat transfer, and species transport simulations were carried out in conjunction with a PCR chemistry model. Our analysis clearly depicts thermo-fluidic and chemical behavior in the device and effectively captures their effects on the device performance of DNA amplification. Through simulation analysis, we have found that fully attached laminar flow dominates in the PCR micro-device. Thermally, the system attains equilibrium at all flow rates considered in this study and the denaturing, annealing and extension channel lengths are sufficient for fluid exiting the channel to reach the temperature set points of PCR. The chemical response of the system is significantly more complex than the thermal response. As expected, the concentration of the dsDNA increases as the sample traverses downstream. The effect of flow rate on dsDNA amplification is significant. At low flow rates, amplification factors close to the ideal are observed whereas at higher flow rates, dsDNA yield exhibits significant non-idealities. This discrepancy is primarily caused by the variations in fluid temperature and residence time of sample species within the channel. Optimal design of the annealing and extension channels is of paramount importance to simultaneously ensure complete reaction, high amplification factor, and high throughput.

Our investigations clearly demonstrate that there are critical design and performance trade-offs associated with the development of microfluidics-based PCR systems. An automated parameterization and optimization methodology based on the computational models developed in the present study can be used to evaluate these trade-offs in a systematic and cost-effective manner. In the future, we will focus on developing an optimization methodology for rational design of microfluidics-based PCR devices.

REFERENCES

[1] G. Hu et. al, Anal.Chimica Acta '06, 557, 146-151, 2006.

[2] J. Kang et. al, *Nanotech'06*, 585-588, Boston, MA.

[3] S. Mehra et. al, *Biotech. Bioeng.* 55, 359-366, 2005.

[4] Z.J. Chen et. al, *Nanotech'01*, 574-577, Hilton Head Island, SC.

[5] http://www.thermalgradient.com

[6] CFD-ACE+ Theory Manual, Version 2006, ESI-CFD, Inc., Huntsville, AL.